CRIMSON PUBLISHERS
Wings to the Research

Determinations in Nanomedicine & Nanotechnology

Research Article

ISSN : 2832-4439

Structural and Magnetic Properties in Sputtered Iron Oxide Epitaxial Thin Films - Magnetite Fe_3O_4 and Epsilon Ferrite ε-Fe_2O_3-

Masato Watanabe*

Research Institute for Electromagnetic Materials, Japan

***Corresponding author:** Masato Watanabe, Research Institute for Electromagnetic Materials, Japan, Email: m_watanabe@denjiken.ne.jp, masato33@innovamateria.jp

submission: February 12, 2019; **Published:** February 21, 2019

Abstract

Epitaxial thin film fabrication of iron oxides including magnetite Fe_3O_4 and epsilon-ferrite ε-Fe_2O_3 with the potential for advancing electromagnetic devices has been investigated, which led to the first ever ε-ferrite epitaxial layer being synthesized in the conventional sputtering process. Concerning Fe_3O_4(100)/MgO (100) films, a cube-on-cube epitaxial relationship and sharp rocking curves with FWHM of 50-350 arcsec were confirmed regardless of the small amount of Ge additions. Sputtering Ar gas pressure PAr heavily influenced their magnetic and transport properties. High P_{Ar}=15m Torr caused a high magnetization of 6.52 kG for the Ge added sample and the clear Verwey transition at 122K for the non Ge addition case. Conversion electron Mössbauer spectroscopy (CEMS) measurements revealed that low P_{Ar}<10m Torr causes Fe/O off-stoichiometry on the oxidizing side for the non Ge addition case and the reductive side for the Ge addition case, respectively. Regarding the α-Fe_2O_3 (001)/$SrTiO_3$ (111) epilayer synthesis, bilayer microstructure composed of an approximately 5nm thick initially grown ε-Fe_2O_3 (001) epilayer and subsequently grown ε-Fe_2O_3(001) epilayer was confirmed from cross-sectional TEM observations. The coexistence of magnetically hard and soft phases was confirmed from the magnetization measurements. As a possible application of the single nm thick ε-Fe_2O_3 layer, 4-resistive-state multiferroic tunnel junction (MFTJ) is considered.

Introduction

Magnetic iron oxides, so-called "ferrites", have been utilized for various electromagnetic applications due to their versatile magnetic properties [1,2] and large natural abundance of main constituent iron and oxygen, which meets recent social requirements for materials such as rare-metal-free ubiquity. Among the huge variety of ferrites, we focused on two iron oxides: magnetite Fe_3O_4 and epsilon ferrite ε-Fe_2O_3, both of which show unique magnetic and electronic functionalities, and attempted to fabricate their epitaxially grown thin films by conventional sputtering, which is an advantageous process for industrial device applications. Magnetite of the first iron oxide is an ubiquitous magnetic material naturally found as the main component of iron sand [3]. Its crystal structure is an inverse spinel that is composed of Fe^{3+} at tetrahedral A sites, Fe^{2+} and Fe^{3+} at octahedral B sites and oxygen sites. It has a room temperature saturation magnetization 4πM of 6.25 kG, which is the highest among iron oxides, and Curie temperature TC of 858 K [4]. Magnetite also shows characteristic electronic properties of half-metallicity [5-8] and large anomalous Hall resistivity ρH ~10-40μΩcm [9], which is comparable with Co based full Heusler compounds [10], leading to the possibility for various spintronic devices such as magnetic tunnel junctions (MTJ). Due to its high biocompatibility, magnetite's biomedical applications such as hyperthermia and drug delivery system (DDS) have also been pursued [11]. To date, our research group conducted research on small-amount element additions in polycrystalline magnetite films and found that the additions of some elements up to several percent, especially Ge, raised their thermal stability and caused an increase in magnetization [12,13]. Since the effects of such element additions in magnetite epifilms have not yet been confirmed, we studied the structural and magnetic effects on small-amount Ge addition to magnetite epifilms in this research.

Epsilon ferrite of the second iron oxide is an emerging hard magnetic material, which has an orthorhombic crystal structure with four iron sites for which magnetic moments are ferrimagnetically aligned [14]. From its high anisotropy field H_A that comes from the high magnetic anisotropy constants of K_a = 7.7 x 10^6 erg/cc along the a axis and K_b = 1.2 x 10^6 erg/cc along the b axis [15] and low magnetization value $4\pi M_S$ = 1.26 kG (=100 emu/cm^3) [16], ε-ferrite shows high resonance frequencies f_r of 35-222 GHz [17,18] and high coercivities over 20 kOe [17,19], leading to the possibility of milli-wave absorption device and magnetic recording media applications. It also shows a rare room-temperature multiferroicity that means simultaneous manifestation of ferromagnetism and ferroelectricity [16], which may have memory or sensor applications as indicated

in the last part of this paper. Its synthesis is difficult due to the characteristics of the metastable phase. Two preparation methods available have been proposed for metastable ε-ferrite so far. One is based on Gibb's energy minimum of ε-ferrite nanoparticles at the particle diameters of 8-30 nm [17], leading to the availability of chemical syntheses of ε-ferrite nanoparticles. The other is based on the constraint of crystal lattices accompanied by epigrowth on certain single-crystalline substrates, which has mainly been conducted for ε-ferrite epifilms by pulsed laser deposition (PLD). A few single-crystalline substrates including $SrTiO_3$(111) [16,20], YSZ (100) [21] and GaN (0001) [22,23] have been reported for the syntheses of ε-ferrite epifilms by PLD. However, epifilm synthesis by conventional sputtering, which is important in industrial applications, has to the best of my knowledge not yet been reported. Therefore, we attempted ε-ferrite epifilm synthesis by RF magnetron sputtering.

Experimental

Sample preparations for both magnetite and ε-ferrite epifilms were done by RF magnetron sputtering. The sputtering target for the magnetite epilayer was a magnetite composite target on which Ge chips were regularly-arrayed and that for the ε-ferrite epilayer was an α-Fe_2O_3 target, respectively. Single-crystalline substrates for epigrowth were polished MgO(100) (Tateho Chemical Industries) for magnetite epilayers and polished $SrTiO_3$(111) (Furuuchi Chemical Corp.) for ε-ferrite epilayers, both of which were heated up to 800°C during deposition after evacuating at less than the vacuum degree of $2x10^{-7}$ Torr. Sputtering gas species were pure Ar gas for magnetite epigrowth and Ar+O_2 mixed gas with the O_2/(Ar +O_2) flow ratio ranging from 25% to 50% for ε-ferrite epigrowth, respectively. Sputtering gas pressures, which strongly affect film characteristics, were varied from 2 to 15 mTorr for magnetite epigrowth, and from 1 to 5 mTorr for ε-ferrite epigrowth, respectively. The film thicknesses for magnetite epilayers ranged from 0.481 μm to 0.548 μm, which were measured by DekTak 150 (Bruker). Ge compositions in magnetite epilayers were evaluated by wavelength dispersive X-ray spectroscopy WDS (INCA WAVE, Oxford Instruments). Structural analyses were conducted using a high-precision X-ray diffractometer with a CuKα radiation, LYNXEYE 1-dimensional detector and Ge (220) monochromator (D8 DISCOVER, Bruker). The film thicknesses of α/ε-Fe_2O_3 bilayers were evaluated by X-ray reflectometry. Magnetization measurements were performed by a superconducting quantum interference device SQUID ($MPMS_3$, Quantum Design) and vibrating sample magnetometer VSM (Tamakawa) with maximum applied fields of 70 kOe and 15 kOe, respectively. Diamagnetic components that come from substrates and sample holders were subtracted from the raw magnetization data. Conversion electron Mössbauer spectroscopy (CEMS) measurement was performed with a 57Co radiation embedded in a Rh matrix, constant-acceleration spectrometer and He-1% $(CH_3)_3CH$ gas-flow counter. Velocity correction was conducted using α-Fe. No ^{57}Fe was doped in the samples for CEMS. All the measurements were performed at room temperature. Resistivity measurements were performed by the 4-point method using PPMS (Quantum Design) in the temperature range of 10-300K. Cross-sectional high-angle annular dark-field scanning transmission electron microscopy (HAADF-STEM) observation (Z-contrast image) and nano beam electron diffraction (NBD) for the α/ε-Fe_2O_3 bilayer were conducted by JEM-ARM200F (200 kV, JEOL).

Results and discussions for Fe_3O_4 epigrowth

A typical θ/2θ scan XRD profile for the 0.6 at%Ge-Fe_3O_4/MgO(100) epifilm is shown in Figure 1. Sharp Fe_3O_4(400) and Fe_3O_4(800) peaks were clearly observed close to the MgO(200) and MgO(400) peaks and no other phase was confirmed, which shows c-axis alignment of the magnetite phase in the direction normal to the film plane. In order to study the effect of sputtering gas pressure P_{Ar} on crystallinity of the magnetite epilayers, full-widths at half maximum (FWHM) of Fe_3O_4(400) rocking curves with varying P_{Ar} are shown in Figure 2 in comparison with FWHM of MgO(200). FWHM of the magnetite epilayers was relatively low ranging from 50 to 350 arcsec, which is the same order of magnitude as those of compound semiconductor epifilms reported so far. The FWHM of magnetite epilayers for $P_{Ar} \leq 7$ mTorr was lower than those for $P_{Ar} \geq 10$ mTorr, indicating that magnetite epilayers with lower $P_{Ar} \leq 7$ mTorr have higher crystallinity than the higher $P_{Ar} \geq 10$ mTorr cases, and shows almost the same crystallinity as those of MgO (200). Conventional θ/2θ scan XRD gives only structural information along the out-of-plane direction, and therefore we conducted Fe_3O_4(311) φ scan XRD that contains its in-plane information, as shown in Figures 3(a) and (b). Different from Fe_3O_4(400), Fe_3O_4(311) is appropriate for φ scan XRD since it is sufficiently separated from the MgO substrate spots in its reciprocal lattice space. Figure 3(c) shows a simulated Fe_3O_4 (311) pole figure with the φ=0° direction along Fe_3O_4[100], of which the inner four spots and outer eight spots correspond to the four peaks in Figure 3(a) and the eight peaks in Figure 3(b), respectively. Reproduction of the simulated pole figure is considered to show the following cube-on-cube orientation relationships: Fe_3O_4[100]//MgO[100], Fe_3O_4[010]//MgO[010] and Fe_3O_4[001]//MgO[001]. We have studied room-temperature magnetic properties for the Fe_3O_4(100)/MgO(100) epifilms varying with Ar sputter gas pressure P_{Ar}. Magnetization curves for P_{Ar}=15 mTorr and P_{Ar}=2 mTorr with the maximum field of 70 kOe are shown in Figures 4(a) and 4(b). Out-of-plane magnetizations for both P_{Ar}=15 mTorr and 2 mTorr exceed the in-plane magnetizations at higher fields over 10 kOe, which suggests the existence of some perpendicular magnetic anisotropy. This large perpendicular anisotropy has been reported for magnetite epifilms and polycrystalline films [24,25] so far and its possible origin is attributed to Out-of-plane moment alignment around antiphase boundaries (APB), which was confirmed by off-axis electron holography [26]. Figure 4(c) summarizes out-of-plane magnetizations 4πM with the maximum applied fields of 15 kOe and 70 kOe for the Ge-doped and non-doped magnetite epifilms as a function of P_{Ar}.

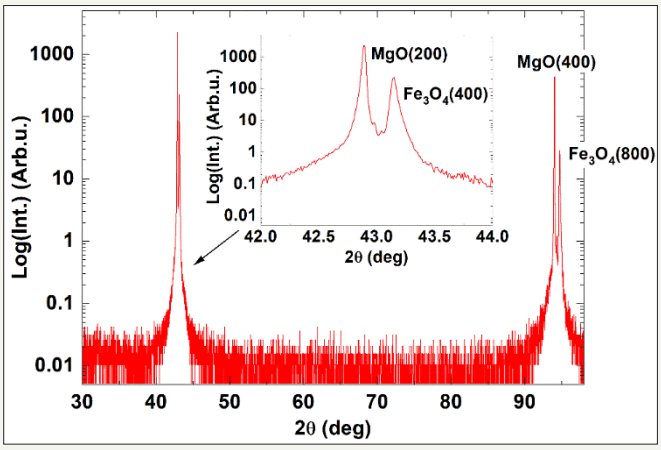

Figure 1: θ/2θ scan XRD profiles for the 0.6 at%Ge added Fe_3O_4 epifilms grown on MgO(100). Magnified profile around MgO(200) and Fe_3O_4(400) peaks is shown in the inset.

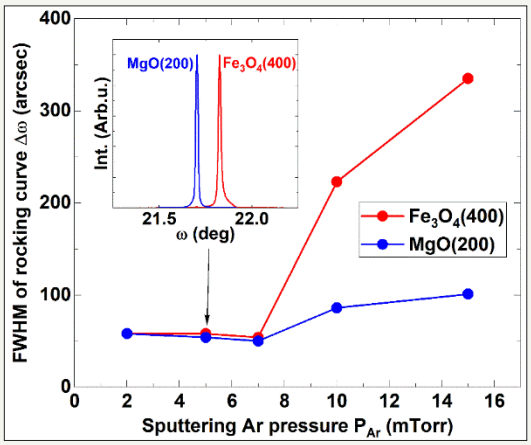

Figure 2: Full widths at half maximum (FWHM) of Fe_3O_4(400) and MgO(200) rocking curves as a function of sputtering Ar pressure P_{Ar} for the Fe_3O_4/MgO (100) epifilms. The inset shows MgO(200) and Fe_3O_4(400) rocking curve profiles for the epifilm at P_{Ar}=5mTorr.

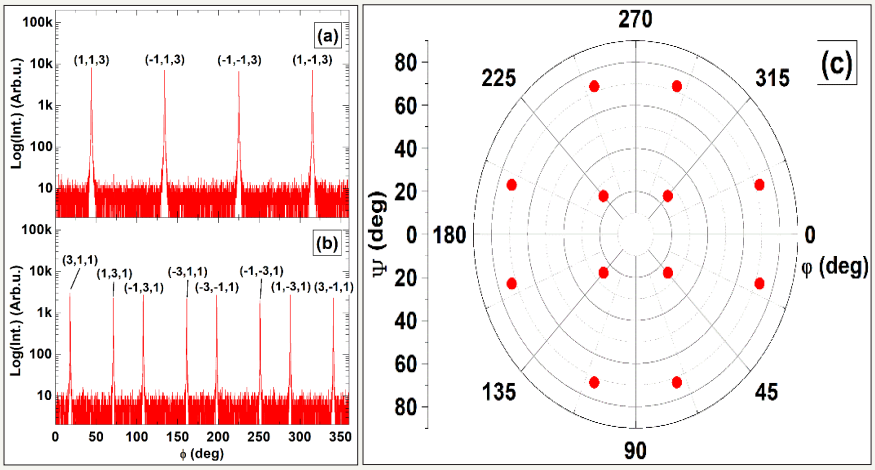

Figure 3: Fe_3O_4(311) φ scan profiles for the Fe_3O_4/MgO(100) epifilms at (a) ψ=25.2393 deg and (b) ψ=72.4512 deg, which correspond to the four inner and eight outer spots in (c) simulated Fe_3O_4 (311) pole figure.

How to cite this article: Masato Watanabe. Structural and Magnetic Properties in Sputtered Iron Oxide Epitaxial Thin Films - Magnetite Fe_3O_4 and Epsilon Ferrite ε-Fe_2O_3-. Determinations Nanomed Nanotechnol. 1(1). DNN.000502. 2019. DOI: 10.31031/DNN.2019.01.000502

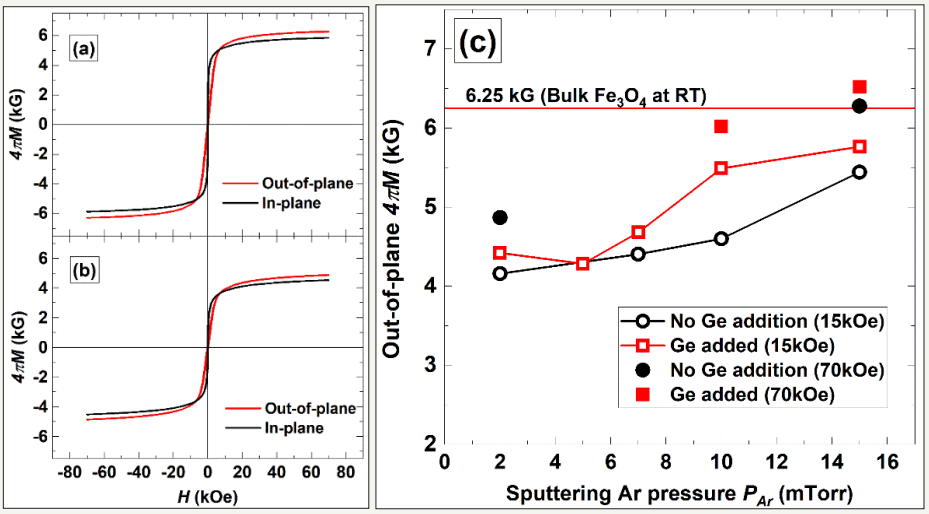

Figure 4: Room-temperature magnetization hysteresis curves for the Fe_3O_4 (100)/MgO(100) epifilms with non Ge addition at (a) P_{Ar}=5 mTorr and (b) P_{Ar}=2 mTorr. The red and black lines stand for out-of-plane and in-plane curves, respectively. (c) Out-of-plane magnetization 4πM at 15 kOe and 70 kOe as a function of sputtering Ar gas pressure P_{Ar}. Red blank squares and black blank circles stand for Ge added and non Ge addition cases at 15 kOe. Solid marks are 4πM at 70 kOe.

For both the Ge-doped and non-doped cases, magnetizations 4πM increase with the increase in P_{Ar}. Moreover, the out-of-plane 4πM for P_{Ar}=15 mTorr is 6.52 kG, which exceeds the 6.25 kG for single crystal magnetite, at the applied field of 70 kOe and still does not saturate at 70 kOe as shown in Figures 4(a) and 4(b). Magnetization enhancement over 12 kG, which is much larger than the bulk value of 6.25 kG, has been reported for 3nm thick magnetite epifilm, the possible origin of which has been attributed to spin flip from ferrimagnetic moment alignment to ferromagnetic type [4]. The same type of enhancement might occur partially for the epifilms as well. In this research, we grew magnetite epifilms at a high substrate temperature of 800°C and magnesium atoms easily diffuse into the magnetite layer [27,28], leading to the possible formation of an interdiffused Mg-Fe_3O_4 layer. Thus, we conducted cross-sectional TEM observation and composition analysis along the out-of-plane direction, which confirmed the existence of a ~100 nm thick Mg-Fe_3O_4 interdiffused layer in the magnetite epifilm with a total thickness of ~500 nm. Mg ferrite $MgFe_2O_4$ has 4πM of 1.149 kG [29], which is much lower than that of the 6.25 kG for magnetite, and so the interdiffused layer is considered to cause a magnetization reduction.

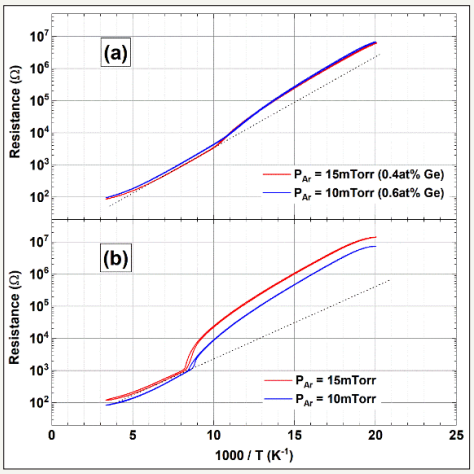

Figure 5: Resistance as a function of 1000/T for (a) the Ge-added and (b) non Ge added Fe_3O_4 (100)/MgO (100) epifilms with sputtering Ar gas pressure P_{Ar}=15 and 10 mTorr.

Since a slight magnetization enhancement was observed for the magnetite epilayer with P_{Ar}=15 mTorr as described above despite the existence of the interdiffused layer, the magnetization enhancement at the undiffused part of magnetite epilayer is considered to be large enough to compensate the magnetization reduction at the Mg interdiffused part. In order to study the Verwey transition, which is sensitive to the film quality and stoichiometry [30], we performed resistance measurements of the (a) Ge-doped and (b) non-doped magnetite epifilms with P_{Ar}=10 and 15 mTorr as a function of the inverse number of temperature 1000/T as shown in Figure 5. The non-doped magnetite epifilms show the clear resistivity change accompanied with the Verwey transition. The transition

How to cite this article: Masato Watanabe. Structural and Magnetic Properties in Sputtered Iron Oxide Epitaxial Thin Films - Magnetite Fe_3O_4 and Epsilon Ferrite ε-Fe_2O_3-. Determinations Nanomed Nanotechnol. 1(1). DNN.000502. 2019. DOI: 10.31031/DNN.2019.01.000502

temperature Tv for P_{Ar}=15 mTorr is 122 K, almost the same as the previously reported value of bulk magnetite. On the contrary, resistivity changes for the Ge-doped samples are diminished and their Tv's decrease until < 100 K. Since the Ge addition also increases the resistivity, the added Ge might be incorporated into B sites with two types of valency and inhibit the hopping conduction. Regardless of the Ge concentrations, we could not observe clear resistivity changes of the Verwey transition for the samples with P_{Ar}<10 mTorr, the magnetizations of which are low as shown in Figure 4(c). For further investigation of magnetism in the magnetite epifilms, we performed CEMS measurements. CEMS spectra for the Ge-added magnetite epifilms are shown in Figure 6(a) P_{Ar}=15 mTorr (0.4 at%Ge) and (b) P_{Ar}=2 mTorr (1.6 at%Ge). The observed spectra can be decomposed into two sharp ferromagnetic sextets that come from tetrahedral A (Fe^{3+}) and octahedral B ($Fe^{2.5+}$) sites. Hyperfine structure parameters, B_{Hf}, δ_{MB} integral intensities for A and B sites and sextet intensity ratios x for the Ge-added magnetite epifilms are summarized in Table 1 in comparison with those of previously reported sputtered magnetite epifilms and natural bulk magnetite [31,32]. The parameters for the P_{Ar}=15 mTorr sample are in good agreement with those of the previously reported film and bulk magnetite. BHf and integral intensities for the P_{Ar}=2 mTorr sample, which has lower magnetization 4πM than the P_{Ar}=15 mTorr sample, deviate from the previously reported values. Sextet intensity ratio x contains information about moment direction according to the following Eq: x= (4 sin2θ)/((1+cos2θ)), where θ stands for the angle between ^{57}Fe magnetic moment and the incident direction of γ-ray for CEMS.

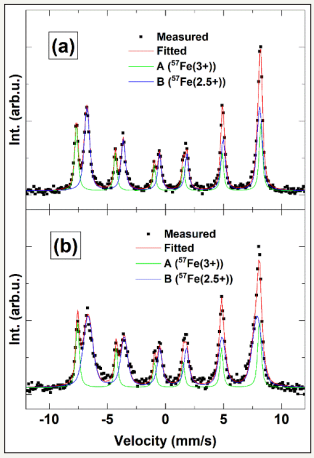

Figure 6: Converson electron Mossbauer spectroscopy (CEMS) spectra for the Fe_3O_4 (100)/MgO(100) epifilms with (a) P_{Ar} = 15 mTorr (0.4 at%Ge) and (b) P_{Ar} = 2 mTorr (1.6 at%Ge). Measured CEMS data (black dots and fitted red lines) are decomposed into A site (green lines) and B site (blue lines) components.

Table 1: Hyperfine structure parameters obtained from CEMS for Fe_3O_4/MgO (100) epifilms with P_{Ar} = 15 mTorr (0.4 at%Ge) and P_{Ar}=2 mTorr (1.6 at%Ge). Previously reported data for sputtered Fe_3O_4 epifilms [31] and natural bulk Fe_3O_4 [32] are also shown for comparison.

	^{57}Fe site	Hyperfine Field B_{hf} (kOe)	Isomer Shift δMB (mm/s)	Integral Intensity Ratio x for A & B Sites (%)	Integral Intensity Ratio x (3:x:1:1:x:3)	4πM (kG)
Fe_3O_4- 0.4at%Ge (15 mTorr)	A (Fe^{3+}) B ($Fe^{2.5+}$)	492 461	0.28 0.67	35.0% 65.0%	1.56	5.8
Fe_3O_4 - l.6at%Ge (2 mTorr)	A (Fe^{3+}) B ($Fe^{2.5+}$)	485 457	0.28 0.64	27.7% 72.3%	1.63	4.5
Sputtered Fe_3O_4 film	A (Fe^{3+}) B ($Fe^{2.5+}$)	491 ± 2 462 ± 2	0.27 ± 0.01 0.67 ± 0.01	33.3 ± 2% 66.6 ± 2%	0.71 - 1.60	4.9 - 6.0
Natural Bulk Fe_3O_4	A (Fe^{3+}) B ($Fe^{2.5+}$)	493 ± 1 460 ± 1	0.27 ± 0.03 0.67 ± 0.03	33.8 ± <2% 66.2 ± <2%	2	

States for x=0 and x=4 mean moment alignments along the out-of-plane and the in-plane directions, respectively. State for x=2 means randomly-oriented or <111> oriented moments. From x<2 for both the P_{Ar}=15 mTorr and 2 mTorr samples, the samples show some perpendicular magnetic anisotropy, which coincides with the feature of magnetization curves in Figures 4(a) and (b). Integral intensity ratios for A and B sites in CEMS contain information about iron vacancy in magnetite. Vacancy parameter δ in $Fe_{3-\delta}O_4$ has the following relation with the ratio of integral intensity for A site to that for B site β : β= (Integral Int. (A site))/(Integral Int. (B site))=((1+5δ))/((2-6δ)) [33]. δ=0 and δ=1/3 correspond to stoichiometric magnetite and stoichiometric γ-Fe_2O_3, respectively. If we take account of the effect of the recoilless fraction, a slight correction to the oxidizing side from β=0.5(δ=0) to

How to cite this article: Masato Watanabe. Structural and Magnetic Properties in Sputtered Iron Oxide Epitaxial Thin Films - Magnetite Fe_3O_4 and Epsilon Ferrite ε-Fe_2O_3-. Determinations Nanomed Nanotechnol. 1(1). DNN.000502. 2019. DOI: 10.31031/DNN.2019.01.000502

β=0.52(δ=4.9x10^{-3}) is required for stoichiometric magnetite [34]. Figures 7(a) and (b) show δ and 4πM at 15 kOe for Ge-doped and non-doped MNT epifilms as a function of P_{Ar}. With the increase in P_{Ar}, δ's approach zero for both the Ge-doped and non-doped samples, which corresponds to the increase in 4πM. Therefore, the 4πM reduction with the decrease in P_{Ar} is considered to be due to the composition deviation from the stoichiometry of magnetite. The vanishing of resistivity change at the Verwey transition with the decrease in P_{Ar} described in the previous part of Figure 5 is considered to be the same as well, and so Fe/O composition deviation is considered to significantly influence the magnetic and transport properties of magnetite.

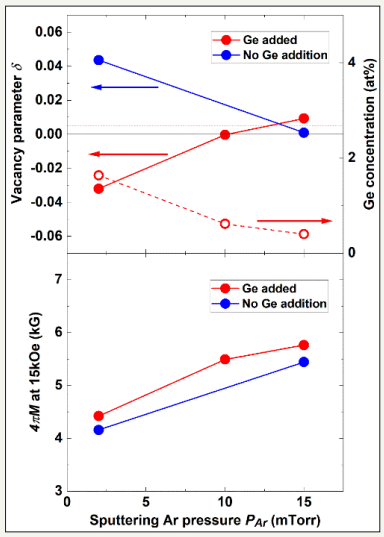

Figure 7: (a) Vacancy parameter δ (solid red circles for Ge added and blue circles for non Ge addition cases) and Ge concentration (blank red circles), and (b) room-temperature magnetization 4πM at 15 kOe for the Fe_3O_4 (100)/MgO(100) epifilms as a function of sputtering Ar pressure P_{Ar}. The ideal δ = +4.9 x 10^{-3} for stoichiometric Fe_3O_4 taking its recoilless fraction into account is indicated with a red dotted line.

Results and discussions for α/ε-Fe_2O_3 bilayer epigrowth

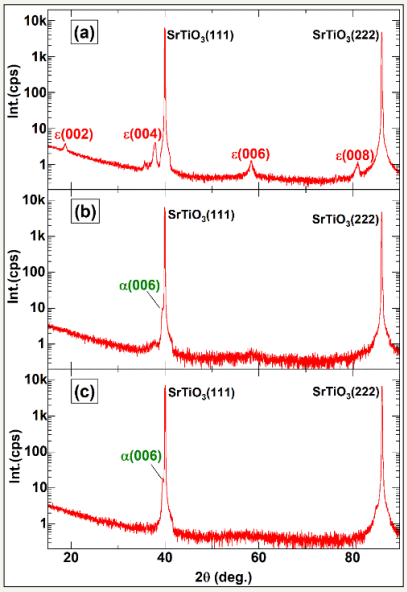

Figure 8: θ/2θ scan XRD profiles for the α- and ε-Fe_2O_3 epifilms grown on $SrTiO_3$(111) with sputtering Ar+25%O_2 mixed gas pressure P(Ar+25%O_2) = (a) 1 mTorr, (b) 2 mTorr and (c) 5 mTorr.

Research on epigrowth of ε-ferrite so far has been mainly focused on the PLD process and the conditions necessary for its epigrowth have been reported to be a high substrate temperature and high oxygen content atmosphere during deposition [16,20-23]. Thus, we conducted sputtered epigrowth deposition at the high substrate temperature of 800ºC with a varying oxygen flow rate ratio Q(O_2)/Q(Ar+O_2). For the no oxygen atmospheric condition, the Fe_3O_4(111) epilayer was grown despite the use of the Fe_2O_3 sputter target and found that ε-ferrite epilayers can be grown in a high oxygen content atmosphere such as the PLD cases as shown

below. This study is the first to report of ε-ferrite epilayer growth by conventional sputtering process. XRD profiles for the Fe_2O_3 epifilms with $Q(O_2)/Q(Ar+O_2)$ =25 % and different sputter gas pressures are shown in Figures 8(a), (b) and (c). A c-axis oriented ε-ferrite epilayer was confirmed only for the lowest gas pressure of a 1 mTorr sample and the higher gas pressure conditions of 2 and 5 mTorr create α-phase epilayers. Low sputter gas pressure causes long mean free paths of sputter particles, leading to high kinetic energies, less collisions and low sputter particle incorporation into the films, which may influence the different phase formation in the epilayers. The prepared film samples on 10 mm square $SrTiO_3$(111) substrates were composed of two different parts of the dark-colored and light-colored areas as shown in the optical images of Figure 9. From XRD with narrowed X-ray beams, the dark-colored and light-colored areas are composed of the c-axis oriented α-phase and ε-phase, respectively. X-ray reflectometry with collimated beams shows that the thicknesses of the dark-colored and light-colored areas are 29 nm and 4 nm, respectively.

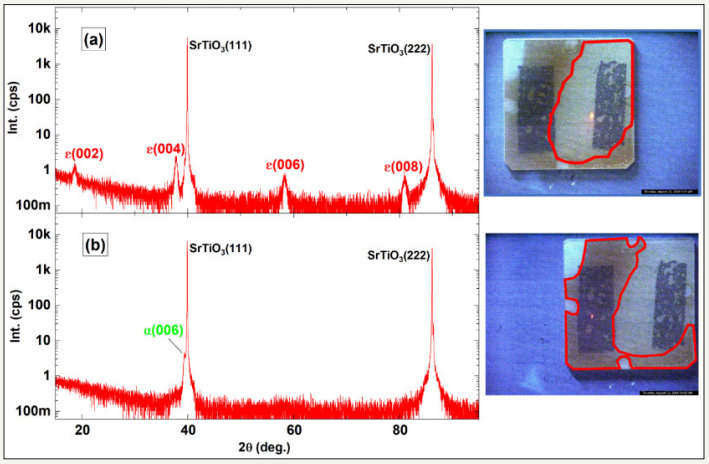

Figure 9: θ/2θ scan XRD profiles for the α- and ε-Fe_2O_3/$SrTiO_3$(111) epifilm (P(Ar+40%O_2) = 1mTorr) in (a) the light-colored area (4nm thick) and (b) the dark-colored area (29nm thick) in the right side sample images (areas surrounded by red lines).

In order to clarify the microstructure of the epilayer, we conducted cross-sectional TEM observations on the dark-colored area of the epifilm with $Q(O_2)/Q(Ar+O_2)$=40% and sputter gas pressure $P(Ar+O_2)$=1 mTorr. Figure 10 shows cross-sectional TEM observation and NBD in the epifilm. It was revealed that the epifilm was composed of two-phase construction where one is α phase of the initial epilayer on the substrate with~5 nm thick and the other is ε-phase of the capped epilayer. From the NBD of Figure 10 (b), both the ε- and α-phase epilayers were aligned with [001] along the out-of-plane direction and [-210] along the in-plane direction. The initial ε-phase epilayer is continuous in this image, however, discontinuous areas were also found to exist from larger area TEM observations.

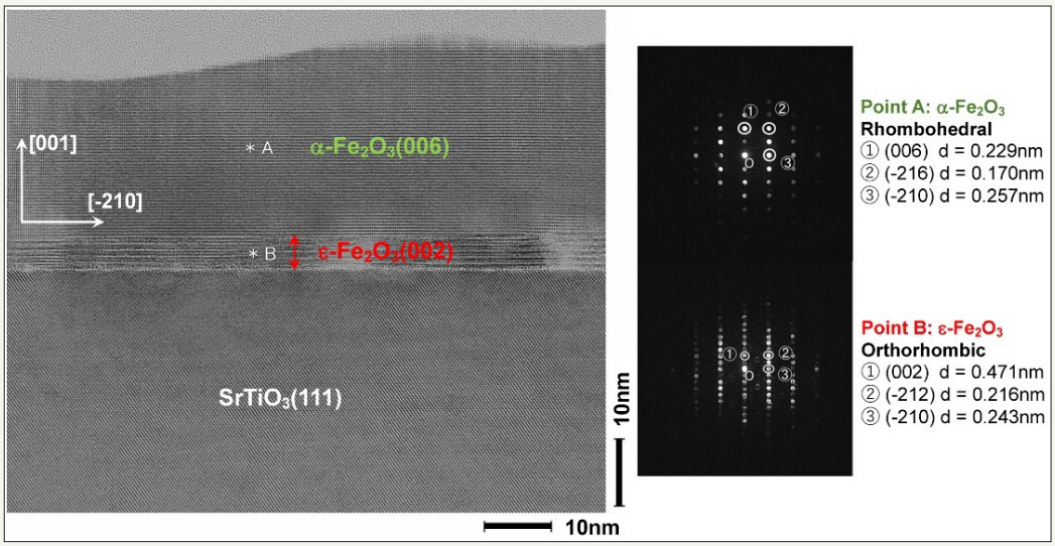

Figure 10: Cross-sectional TEM image and nano beam electron diffraction (NBD, point A and B in the TEM image) for the α- and ε-Fe_2O_3/$SrTiO_3$(111) epifilm (P(Ar+40%O_2)=1mTorr) in the dark-colored area shown in Figure 9.

How to cite this article: Masato Watanabe. Structural and Magnetic Properties in Sputtered Iron Oxide Epitaxial Thin Films - Magnetite Fe_3O_4 and Epsilon Ferrite ε-Fe_2O_3-. Determinations Nanomed Nanotechnol. 1(1). DNN.000502. 2019. DOI: 10.31031/DNN.2019.01.000502

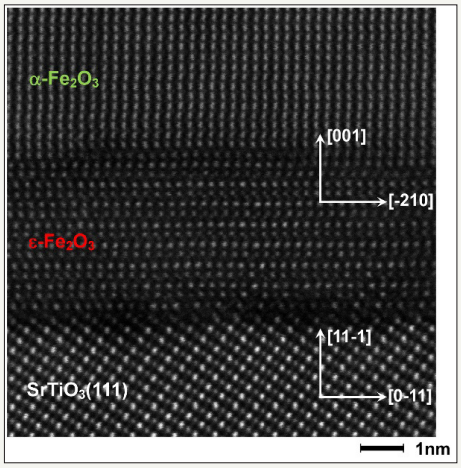

Figure 11: Cross-sectional HAADF-STEM (Z-contrast) image for the α/ε-Fe_2O_3/$SrTiO_3$(111) epifilm (P(Ar+40%O_2) = 1mTorr) in the dark-colored area shown in Figure 9.

Since a clear lattice image was confirmed in Figure 10, we also conducted HAADF-STEM observation with higher magnification as shown in Figure 11. Within the scope of our TEM observation, no crystalline boundaries were confirmed in the ε-phase epilayer though some disorder of atomic arrangement was observed, which is different from the case of the previously reported ε-phase epilayer prepared by PLD. It has been reported that PLD can create a thicker c-axis oriented ε-phase epilayer up to about 100nm thick and the PLD epilayer is composed of nano-sized crystal domains with the in-plane crystal orientation of six-fold symmetry [20]. ε-ferrite has been mainly studied within the form of nanoparticles and its phase formation is explained by free energy minimum at the diameters of 8-30nm [17]. However, other forms of epitaxially grown ε-ferrite have also been reported such as nanowire or nanobelt several micrometers in length by PLD [35,36] and peculiar dendritic microstructures of mullite on the scale of several micrometers in Japanese stoneware, Bizen-yaki [37,38].

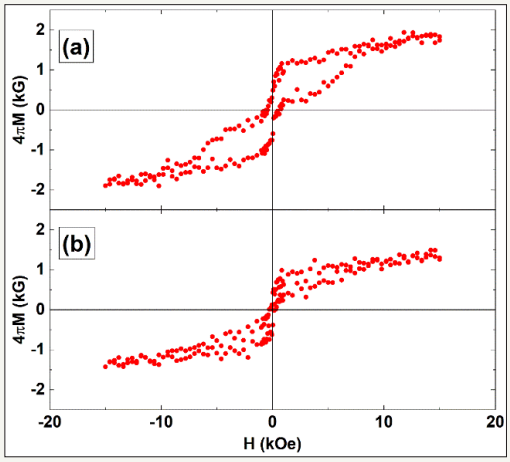

Figure 12: Room-temperature in-plane magnetization curves for the α- and ε-Fe_2O_3/ $SrTiO_3$(111) epifilm (P(Ar+40%O_2)=1mTorr) with total thicknesses = (a) 121 nm and (b) 29 nm. Magnetizations 4πM were evaluated assuming 5nm thickness of the ε-Fe_2O_3 initial epilayer.

Therefore, further study is considered to be necessary regarding the generation mechanism of ε-ferrite. Room temperature magnetic properties of the two phase α/ε-Fe_2O_3 epilayer with different total thicknesses were investigated as shown in Figure 11. The hysteresis curves show that the sample was composed of decoupled magnetically soft and hard phases. The hard phase comes from original hard ε-ferrite and the soft phase comes from ε-ferrite in which magnetic anisotropy was diminished by some imperfections of crystallinity since no other magnetic phase could be confirmed. The magnetization values obtained by assuming 5 nm thick ε-ferrite epilayers had mostly good agreement with the reported value of 1.26 kG in ε-ferrite by the same order of magnitude, which is consistent with the above TEM observation results. As a possible application of such single nm-scale ε-ferrite epilayer, it may be applied to the multiferroic barrier in multiferroic tunnel junction (MFTJ). Spin filter MFTJ with half-metallic and multiferroic perovskite oxides was firstly reported by a French group in 2007 as a prototype of the 4-resistive-state memory that utilizes both tunnel magnetoresistance (TMR) and tunnel electro resistance (TER) effects [39,40]. 4-resistive states in MFTJ correspond to the

How to cite this article: Masato Watanabe. Structural and Magnetic Properties in Sputtered Iron Oxide Epitaxial Thin Films - Magnetite Fe_3O_4 and Epsilon Ferrite ε-Fe_2O_3-. Determinations Nanomed Nanotechnol. 1(1). DNN.000502. 2019. DOI: 10.31031/DNN.2019.01.000502

configurations of magnetic moment M and electric polarization P as shown in Figure 12. Because the high-temperature phase of magnetite and ε-ferrite shows half-metallicity and multiferroicity at room temperature, respectively, we anticipated that all ferrite MFTJ would work at room-temperature if it were composed of a magnetite electrode and ε-ferrite barrier as shown in Figure 12. In order to secure the independent switching function of 4-state memory, ME coupling between M and P in the multiferroic barrier should not be strong and so the clarification of magnitude of ME coupling in ε-ferrite is required. A study on optical ME coupling in ε-ferrite utilizing its second harmonic generation SHG effect showed that it has a strong ME coupling from the magnetic component of SHG [15], thus it might be necessary to control the magnitude of coupling by measures such as some element additions in order to realize 4-resistive-state magnetite/ε-ferrite MFTJ.

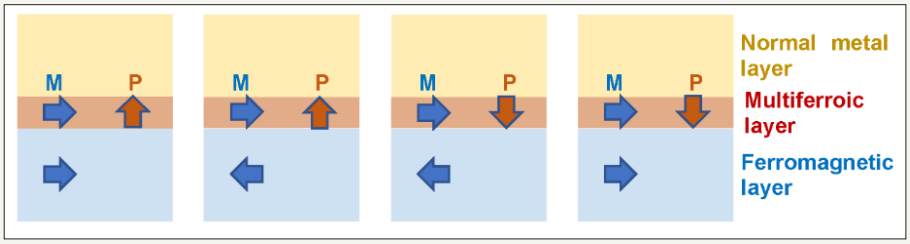

Figure 13: Schema of 4-resistive-state multiferroic tunnel junction (MFTJ) utilizing the spin filter effect in multiferroic barrier such as ε-Fe_2O_3 thin layer and tunnel electro resistance (TER) effect. M and P represent magnetic moment and electric polarization, respectively.

Summary

Epitaxial growth of magnetite and ε-ferrite was conducted by conventional RF magnetron sputtering on MgO(100) and $SrTiO_3$(111), respectively. Fe_3O_4/MgO(100) epifilms have a cube-on-cube epitaxial relationship and a high crystallinity was confirmed from the sharp rocking curves with FWHM of 50-350 arcsec for both the Ge-added and non Ge addition cases. Sputtering Ar gas pressure P_{Ar} significantly influenced their magnetic and transport properties. The magnetite epifilm for P_{Ar}=15 mTorr had a high magnetization of 6.52 kG for the Ge added case and the clear Verwey transition at 122 K for the non Ge addition case.

CEMS measurements revealed that low P_{Ar} < 10 mTorr causes Fe/O off-stoichiometry on the oxidizing side for the non Ge addition case and the reductive side for the Ge addition case, respectively. Regarding ε-Fe_2O_3 epilayer synthesis, bilayer microstructure composed of an approximately 5nm thick ε-Fe_2O_3(001) epilayer initially grown on $SrTiO_3$(111) and a subsequently grown α-Fe_2O_3 (001) epilayer was confirmed from cross-sectional TEM observations. The coexistence of magnetically hard and soft phases was confirmed from the magnetization measurements. As a possible application of the single nm thick ε-Fe_2O_3 layer, 4-resistive-state multiferroic tunnel junction (MFTJ) could be considered.

Acknowledgement

This article was supported by JSPS KAKENHI Grant number 17K06806, "Magnetic anisotropy control by coherency strain in element-added magnetite thin films" and partially presented at 2nd International Conference on Magnetism and Magnetic Materials, Budapest, Hungary in September 24-26, 2018 (Allied Academies). I thank Dr. S. Abe, President K. Arai of Research Institute for Electromagnetic Materials, Prof. S. Sugimoto and Prof. K. Takanashi of Tohoku Univ. for their beneficial discussions, and also thank Dr. M. Ikeda of Quantum Design Japan, Ms. A. Tsutsui of Foundation for Promotion of Material Science and Technology of Japan (MST), Dr. T. Segi of KOBELCO Research Institute and Mr. H. Sato of Research Institute for Electromagnetic Materials for their assistance with and discussions on the characterizations.

References

1. Goldman A (2006) Modern Ferrite Technology 2nd Edition, Springer Science+Business Media Inc, New York, USA.
2. Tartaj P, Morales MP, Gonzalez-Carreño T, Veintemillas-Verdaguer S, Serna CJ (2011) The iron oxides strike back: From biomedical applications to energy storage devices and photoelectrochemical water splitting. Adv Mater 23(44): 5243-5249.
3. Fahlepy MR, Tiwow VA, Subaer (2018) Characterization of magnetite (Fe_3O_4) minerals from natural iron sand of Bonto Kanang Village Takalar for ink powder (toner) application. J Phys: Conf Ser 997012036.
4. Arora SK, Wu HC, Choudhary RJ, Shvets IV, Mryasov ON, et al. (2008) Giant magnetic moment in epitaxial Fe_3O_4 thin films on MgO (100). Phys Rev B 77(13): 134443.
5. Yanase A, Siratori K (1984) Band structure in the high temperature phase of Fe_3O_4. J Phys Soc Jpn 53(1): 312-317.
6. Fonin M, Dedkov YS, Pentcheva R, Rüdiger U, Güntherodt G (2007) Magnetite: A search for the half-metallic state. J Phys: Condens Matter 19(31): 315217.
7. Wang W, Mariot JM, Richter MC, Heckmann O, Ndiaye W, et al. (2013) Fe t_{2g} Band dispersion and spin polarization in thin films of Fe_3O_4 (001)/MgO (001): Half-metallicity of magnetite revisited. Phys Rev B 87(8): 085118.
8. McKenna KP, Hofer F, Gilks D, Lazarov VK, Chen C, et al (2014) Atomic-scale structure and properties of highly stable antiphase boundary defects in Fe_3O_4. Nat Commun 5: 5740.
9. Fernández PA, De Teresa JM, Orna J, Morellon L, Algarabel PA, et al. (2008) Universal scaling of the anomalous Hall effect in Fe_3O_4 epitaxial thin films. Phys Rev B 77(10): 100403(R).
10. Tung JC, Guo GY (2013) High spin polarization of the anomalous Hall current in Co-based Heusler compounds. New J Phys 15: 033014.
11. Ito A, Shinkai M, Honda H, Kobayashi T (2005) Medical application of functionalized magnetic nanoparticles. J Biosci Bioeng 100(1): 1-11.

12. Abe S, Ohnuma S (2008) Magnetite thin films containing a small amount of Ge. Appl Phys Express 1(11): 111304.

13. Abe S, Ping DH, Ohnuma M, Ohnuma S (2011) Selective product of magnetite through addition of small amount of metal element. Jpn J Appl Phys 50(6R): 063002.

14. Gich M, Frontera C, Roig A, Taboada E, Molins E (2006) High and low-temperature crystal and magnetic structures of ε -Fe_2O_3 and their correlation to its magnetic properties. Chem Mater 18(16): 3889-3897.

15. Ohkoshi S, Namai A, Imoto K, Yoshikiyo M, Tarora W, et al. (2015) Nanometer-size hard magnetic ferrite exhibiting high optical-transparency and nonlinear optical-magnetoelectric effect. Sci Rep 5: 14414.

16. Gich M, Fina I, Morelli A, Sánchez F, Alexe M, et al. (2014) Multiferroic Iron Oxide thin films at room temperature. Adv Mater 26(27): 4645-4652.

17. Tuček J, Zbořil R, Namai A, Ohkoshi S (2010) ε-Fe_2O_3: An advanced nanomaterial exhibiting giant coercive field, millimeter-wave ferromagnetic resonance, and magnetoelectric coupling. Chem Mater 22(24): 6483-6505.

18. Namai A, Yoshikiyo M, Yamada K, Sakurai S, Goto T, et al. (2012) Hard magnetic ferrite with a gigantic coercivity and high frequency millimetre wave rotation. Nat Commun 3: 1035.

19. Ohkoshi S, Sakurai S, Jin J, Hashimoto K (2005) The addition effects of alkaline earth ions in the chemical synthesis of ε-Fe_2O_3 nanocrystals that exhibit a huge coercive field. J Appl Phys 97(10): 10K312.

20. Gich M, Gazquez J, Roig A, Crespi A, Fontcuberta J, et al. (2010) Epitaxial stabilization of ε-Fe_2O_3 (00l) thin films on $SrTiO_3$ (111). Appl Phys Lett 96(11): 112508.

21. Corbellini L, Lacroix C, Harnagea C, Korinek A, Botton GA, et al. (2017) Epitaxially stabilized thin films of ε-Fe_2O_3 (001) grown on YSZ (100). Sci Rep 7(1): 3712.

22. Ukleev V, Suturin S, Nakajima T, Arima T, Saerbeck T, et al. (2018) Unveiling structural, chemical and magnetic interfacial peculiarities in ε-Fe_2O_3/GaN (0001) epitaxial films. Sci Rep 8: 8741.

23. Suturin SM, Korovin AM, Gastev SV, Volkov MP, Sitnikova AA, et al. (2018) Tunable polymorphism of epitaxial iron oxides in the four-in-one ferroic-on-GaN system with magnetically ordered α-, γ-, ε-Fe_2O_3, and Fe_3O_4 layers. Phys Rev Materials 2: 073403.

24. Hibma T, Voogt FC, Niesen L, van der Heijden PAA, et al. (1999) Anti-phase domains and magnetism in epitaxial magnetite layers. J Appl Phys 85(8): 5291-5293.

25. Watanabe M, Abe S (2016) Out-of-plane magnetic moment and lattice distortion in sputtered Ge added Fe_3O_4 thin film. J Nanosci Nanotechnol 16(3): 2509-2516.

26. Kasama T, Dunin-Borkowski RE, Eerenstein W (2006) Off-axis electron holography observation of magnetic microstructure in a magnetite (001) thin film containing antiphase domains. Phys Rev B 73(10): 104432.

27. Shaw KA, Lochner E, Lind DM (2000) Interdiffusion study of magnesium in magnetite thin films grown on magnesium oxide (001) substrates. J Appl Phys 87(4): 1727-1733.

28. Kim-Ngan N-TH, Balogh AG, Meyer JD, Brötz J, Zając M, et al. (2009) Thermal and irradiation induced interdiffusion in magnetite thin films grown on magnesium oxide (001) substrates. Surf Sci 603(9): 1175-1181.

29. Patil SH, Patil SI, Kadam SM, Chougule BK (1992) Magnetization and structural studies of $CuxMg1-xFe_2O_4$ ferrite system. J Mag Mater 110(1-2): 147-150.

30. Aragón R, Rasmussen RJ, Shepherd JP, Koenitzer JW, Honig JM (1986) Effect of stoichiometry changes on electrical properties of magnetite. J Mag Mater 54-57(3): 1335-1336.

31. Margulies DT, Parker FT, Spada FE, Goldman RS, Li J, et al. (1996) Anomalous moment and anisotropy behavior in Fe_3O_4 films. Phys Rev B 53(14): 9175-9187.

32. Evans BJ, Hafner SS (1969) 57Fe Hyperfine fields in magnetite (Fe_3O_4). J Appl Phys 40(3): 1411-1413.

33. Voogt FC, Fujii T, Smulders PJM, Niesen L, James MA, et al. (1999) NO_2-Assisted molecular-beam epitaxy of Fe_3O_4, Fe_3-δO_4, and γ-Fe_2O_3 thin films on MgO (100). Phys Rev B 60(15): 11193-11206.

34. Da Costa GM, Blanco-Andujar C, De Grave E, Pankhurst QA (2014) Magnetic nanoparticles for in vivo use: A critical assessment of their composition. J Phys Chem B 118(40): 11738-11746.

35. Morber JR, Ding Y, Haluska MS, Li Y, Liu JP, et al. (2006) PLD-Assisted vls growth of aligned ferrite nanorods, nanowires, and nanobelts-synthesis, and properties. J Phys Chem B 110(43): 21672-21679.

36. Ding Y, Morber JR, Snyder RL, Wang ZL (2007) Nanowire structural evolution from Fe_3O_4 to ε-Fe_2O_3. Adv Funct Mater 17(7): 1172-1178.

37. Kusano Y, Fujii T, Takada J, Fukuhara M, Doi A, et al. (2008) Epitaxial growth of ε-Fe_2O_3 on mullite found through studies on a traditional Japanese stoneware. Chem Mater 20(1): 151-156.

38. Kusano Y, Fukuhara M, Takada J, Doi A, Ikeda Y, et al. (2010) Science in the Art of the Master Bizen Potter. Acc Chem Res 43(6): 906-915.

39. Gajek M, Bibes M, Fusil S, Bouzehouane K, Fontcuberta J, et al. (2007) Tunnel junctions with multiferroic barriers. Nat Mater 6: 296-302.

40. Yin Y, Li Q (2017) A review on all-perovskite multiferroic tunnel junctions. J Materiomics 3(4): 245-254.